

The direct midpoint method as a quantum mechanical integrator

Ulrich Mutze *

A computational implementation of quantum dynamics for an arbitrary time-independent Hamilton operator is defined and analyzed. The proposed evolution algorithm for a time step needs three additions of state vectors, three multiplications of state vectors with real numbers, and one application of the square of the Hamilton operator to a state vector. A trajectory starting from a unit-vector remains totally within the unit-sphere in Hilbert space if the time step is smaller than 2 divided by the norm of the Hamilton operator. If the time step is larger than this bound, the trajectory grows exponentially over all limits.

The method is exemplified with a computational quantum system which models collision and inelastic scattering of two particles. Each of these particles lives in a discrete finite space which is a subset of a line. The two lines thus associated with the particles cross each other at right angle.

1 Introduction

The last few decades have seen an ever-strengthening interaction of physics, mathematics, and computing. *Object oriented programming languages* have provided new means for defining models of physical systems. These *computational models* are as natural or as artificial as are the traditional models involving, for instance, differential manifolds and differential equations. Unlike the traditional models, they can be *executed* on a computer to produce results automatically which transcend the limitations of human attentiveness. Object oriented programming languages are *formal languages* just as those on which *Mathematical Logic* is based today. They incorporate a fair amount of experience on formalizing real-world situations and provide methods for abstraction and comprehension which are similar in intent and structure to *categories* and *functors* in mathematics and to the idealizations that constitute *theories* in physics. In languages in which execution of a program has to be preceded by compilation (as, for instance, in

*ulrichmutze@aol.com (may change) thus also: Am Bahndamm 22, 73342 Bad Ditzenbach, Germany, phone ++ 49 (0) 7335 5786

C++) this procedure provides a check of syntactical correctness which is hard to obtain for models formulated in the traditional framework of mathematical physics.

Each kind of mathematical object to be used in the following has been represented in C++ in a way that working with these objects in programs involves not much more key strokes than placing them on paper. For instance, the algorithm (38) can be formulated as follows in my C++ class system ¹ :

```
R tau=0.5*dt;
t+=tau;
psi+=phi*tau;
phi+=psi.dot().dot()*dt;
psi+=phi*tau;
t+=tau;
```

In an epoch that just learns to use quantum dynamics to implement computers (quantum computers) we are in a position to enjoy the observation that computational models of the quantum world (and of quantum computers in particular) can be based on classical computation where data can be stored at addressable locations (registers) in binary format and where register states are *not* subjected to quantum interference.

2 A simple framework for computational quantum mechanics

Some introductions to quantum mechanics present the Heisenberg commutation relations (canonical commutation relations) as a constitutive element of the theory. From the simple fact that each commutator of finite matrices has trace zero, and thus can't be equal to any non-zero multiple of the unit-matrix, one has an argument in favor of quantum mechanical state spaces being infinite-dimensional. That this is a misleading argument should become clear from the present article which treats quantum dynamics in finite dimensional state spaces.

Let us recall the basic facts on operators in a general n -dimensional complex Hilbert ² space \mathcal{H} ($n \in \mathbb{N}$) and their relation to quantum theory in the simplified form which results from the finiteness of dimension. Quantum mechanical models with state space \mathcal{H} can be defined in terms of linear operators in \mathcal{H} and their interpretation as idealized measurement devices, or as generators of symmetries. In accordance with this, there are three important classes of operators: *self-adjoint* operators (i.e. the linear operators A satisfying $A^* = A$) to represent measurement devices (observables), *skew-adjoint* operators (i.e. the linear operators A satisfying $A^* = -A$) to represent generators of symmetries, and *unitary* operators (i.e. the linear operators A satisfying $AA^* = A^*A = \mathbf{1} := \text{identity}$) to represent symmetries. Of course, the *adjoint* A^* of a linear operator A is defined by $\langle A\psi|\phi\rangle = \langle\psi|A^*\phi\rangle$ for all $\psi, \phi \in \mathcal{H}$, where $\langle\psi|\phi\rangle$ denotes the *scalar product* ³ of

¹I'm open to provide source code to interested readers.

²Historically, Hilbert's name is associated with the infinite-dimensional case only, but it is very convenient to have a common name for both cases.

³assumed to be a linear function of the second argument and a semi-linear function of the first one

ψ and ϕ . The adjoint cooperates with the natural algebraic structure of linear operators: $(zA)^* = \bar{z}A^*$, $(A+B)^* = A^* + B^*$, $(AB)^* = B^*A^*$ and satisfies $A^{**} = A$. Since the dimension of \mathcal{H} is finite, we have $AB = \mathbf{1} \Leftrightarrow BA = \mathbf{1} \Leftrightarrow A = B^{-1} \Leftrightarrow B = A^{-1}$. For each skew-adjoint A , the operator $\exp(A) := \sum_{k=0}^{\infty} A^k/k!$ is unitary and the mapping $\mathbb{R} \ni t \mapsto \exp(tA)$ defines the ‘unitary one-parameter group’ generated by A . Any operator A belonging to one of these kinds is *normal* (i.e. $AA^* = A^*A$) and thus has a family $(e_i)_{i=1}^n$ of n orthonormal eigenvectors: $Ae_i = a_i e_i$, $\langle e_i | e_j \rangle = \delta_{ij}$, $a_i \in \mathbb{C}$. Any such pair $(e_i)_{i=1}^n$, $(a_i)_{i=1}^n$ is said to be a *spectral decomposition* of A and the a_i are said to be eigenvalues of A . The set $\sigma(A) := \{a_i : i \in \{1, \dots, n\}\}$ is said to be the *spectrum* of A , and for each $a \in \sigma(A)$, the linear space spanned by the corresponding eigenvectors $\{e_i : a = a_i\}$ is said to be the *eigenspace* of a and its dimension the *multiplicity* of a . A is self-adjoint iff all its eigenvalues are real; iff all eigenvalues belong to $\{0, 1\}$ it is said to be a *projector*. Equivalently, projectors can be defined as those self-adjoint operators A which satisfy $AA = A$. Notice that, for a self-adjoint A , the ‘imaginary multiple’ iA is skew-adjoint and vice versa. For example, the observable H of total energy gives rise to the generator $\frac{i}{\hbar}H$ of the one-parameter group of time-translations. With any two vectors ψ, ϕ one associates the linear operator $|\psi\rangle\langle\phi|$ which maps any χ to $\langle\phi|\chi\rangle\psi$. It is sometimes called the *dyadic product* of ψ and ϕ . The adjoint of $|\psi\rangle\langle\phi|$ is easily seen to be $|\phi\rangle\langle\psi|$. Thus the dyadic product of two non-vanishing vectors is normal iff these vectors are proportional to each other. For each unit-vector ψ (i.e. $\|\psi\| = 1$, where $\|\psi\| := \sqrt{\langle\psi|\psi\rangle}$), the operator $|\psi\rangle\langle\psi|$ is a projector. For any linear operator A , one defines $\|A\| := \text{Max}\{\|A\psi\| : \psi \in \mathcal{H}, \|\psi\| = 1\}$. For a normal operator A with a spectral decomposition $(e_i)_{i=1}^n$, $(a_i)_{i=1}^n$, one has $\|A\| = \text{Max}\{|a_i| : i \in \{1, \dots, n\}\}$ and $A = \sum_{i=1}^n a_i |e_i\rangle\langle e_i| = \sum_{a \in \sigma(A)} a E_a^A$, where $E_a^A := \sum_{i \in \{i : a_i = a\}} |e_i\rangle\langle e_i|$. The function $\sigma(A) \ni a \mapsto \langle\psi|E_a^A\psi\rangle$ defines the *distribution* of A -values in state ψ , $\|\psi\| = 1$. It determines an atomic measure on \mathbb{C} , which for self-adjoint A is entirely concentrated in \mathbb{R} . For a self-adjoint operator A , the function

$$Q_A : \mathcal{H} \rightarrow \mathbb{R}, \quad \psi \mapsto \frac{\langle\psi|A\psi\rangle}{\langle\psi|\psi\rangle} \quad (1)$$

is continuous and the range $Q_A(\mathcal{H})$ is a closed interval (which may be a single point), which contains all eigenvalues of A , and the boundaries of which are eigenvalues of A . For each boundary point r of this interval, the inverse image $Q_A^{-1}(r)$ consists of eigenvectors of A with eigenvalue r .

Who feels relief that there are no problems with unbounded operators and with spectral sets that don’t consist of eigenvalues, be warned. These difficult guests come here in disguise: The eigenvalues of an operator may differ by many orders of magnitude and so may the distances between eigenvalues. The difficulties then become apparent when it comes to computation.

In the present article, finite-dimensional state spaces result from discretization of the part of physical space in which an idealized physical system ‘lives’ in the sense that its states can be represented as complex-valued wave functions which depend on one or more variables that take values in this part of space. This part of space will be referred to as the *biotope* of the system.

This discretization of the biotope is used in a similar spirit as it is employed for the numerical solution of partial differential equations or for the computational analysis of technical (and natural) systems by means of the *finite element method* (FEM). It should not be excluded that physical space is discrete per se. However, this is certainly not relevant for systems that can be described by non-relativistic quantum mechanics. Even with discretized space, there needs no fixed limit on the number of points to be set in a computational model. Dynamically allocated arrays support this in all modern programming languages. If such models make non-trivial use of their freedom, and increase the number of state components from time step to time step in a dynamical simulation, the computation time will also grow from step to step unless the computer grows too (just as the universe is reported to do).

We may represent the discretized biotope by any finite set I . For any such set, we define the Hilbert space $\mathcal{H}(I, \mathbb{C})$ as the set of \mathbb{C} -valued, I -indexed lists $\psi = (\psi_i)_{i \in I}$, endowed with the natural \mathbb{C} -linear structure, and with the scalar product $\langle \psi | \phi \rangle := \sum_{i \in I} \bar{\psi}_i \phi_i$. The dimension of this space is obviously given by the number $|I|$ of elements of I . Lists with user-defined types of index and value are well supported in C++ as a template class `map<IndexType, ValueType>`, which allowed me to code quantum dynamics in Fock space very compactly. For each linear operator A in $\mathcal{H}(I, \mathbb{C})$, there is a \mathbb{C} -valued family $(A_{i i'})_{i, i' \in I}$ such that

$$(A\psi)_i = \sum_{i' \in I} A_{i i'} \psi_{i'} \quad \text{for all } \psi \in \mathcal{H}(I, \mathbb{C}), i \in I. \quad (2)$$

If the indexing of discrete positions is done reasonably, and A is an operator with physical meaning, only a few i' will contribute to this sum for a given i . The set I needs to carry an arithmetical structure that allows finding these contributions by means of an algorithm. An important special case is that there is a map $\iota : I \rightarrow I$ such that $A_{i i'} = \delta_{\iota(i) i'}$ and hence

$$(A\psi)_i = \psi_{\iota(i)} \quad \text{for all } \psi \in \mathcal{H}(I, \mathbb{C}), i \in I. \quad (3)$$

Such a linear operator A is sometimes said to be *induced* by ι , and ι is said to be the *inducing map* of A . It is easy to see that an induced operator is unitary iff its inducing map is bijective. Obviously, the inverse U^{-1} of an induced unitary operator U is induced by the inverse of the inducing map of U . We get an injective group homomorphism, when we assign to each permutation of I the unitary operator that is induced by it.

For Hilbert spaces of this form $\mathcal{H}(I, \mathbb{C})$, the definition of *tensor products* is canonical:

$$\begin{aligned} \mathcal{H}(I, \mathbb{C}) \otimes \mathcal{H}(J, \mathbb{C}) &:= \mathcal{H}(I \times J, \mathbb{C}), \\ (\psi \otimes \phi)_{ij} &:= \psi_i \phi_j \quad \text{for all } \psi \in \mathcal{H}(I, \mathbb{C}), \phi \in \mathcal{H}(J, \mathbb{C}), i \in I, j \in J. \end{aligned} \quad (4)$$

Let A and B be linear operators in $\mathcal{H}(I, \mathbb{C})$ and $\mathcal{H}(J, \mathbb{C})$ respectively. Then one defines the linear operator $A \otimes B$ in $\mathcal{H}(I \times J, \mathbb{C})$ as

$$((A \otimes B)\psi)_{ij} := \sum_{i' \in I, j' \in J} A_{i i'} B_{j j'} \psi_{i' j'} \quad \text{for all } \psi \in \mathcal{H}(I \times J, \mathbb{C}), i \in I, j \in J. \quad (5)$$

Since $I \times J$ is again a finite set, one may iterate this construction to arrive at a quantum mechanical system with many subsystems⁴.

From a computational point of view, there is a close analogy between the discreteness of the biotope and the discreteness of the values which a wave function can take at these discrete positions. Every computational model which uses the built-in numbers of a programming language, replaces the mathematical real or complex numbers by a finite surrogate in which the arithmetic laws hold only up to numerical noise. In an object oriented language one is free to replace the built-in numbers by any implementation of floating point numbers of arbitrary storage size or even of dynamical storage size. In the latter case, the number of bits needed to hold the value of a variable grows from multiplication to multiplication. When used naively, such numbers will overload the most capable computer before it arrived at the solution of any non-trivial computation. Taking this into account, one may recognize computer numbers⁵ of fixed storage size as not fundamentally inferior to the celebrated complete topological field \mathbb{R} .

In this section we will treat systems in one spatial dimension. The demonstration system in Section 5 will be defined in terms of a tensor product of two such systems. In order to express one-dimensionality in space, we use for the previously introduced index set I the following arithmetical model of a discrete space with n elements

$$\mathbb{Z}_n := \{0, \dots, n-1\}, \quad n \in \mathbb{N}, \quad n > 0 \quad (6)$$

equipped with the operation

$$\oplus : \mathbb{Z}_n \times \mathbb{Z} \rightarrow \mathbb{Z}_n, \quad i \oplus s := \text{remainder of the division } (i+s)/n, \quad (7)$$

of *addition modulo n* and the operation

$$\rho : \mathbb{Z}_n \rightarrow \mathbb{Z}_n, \quad i \mapsto n-1-i \quad (8)$$

of *reflection*. This is a special case of the general situation that there is a *group* (here an extension of the the additive group \mathbb{Z} by a reflection) which acts as a transformation group on a carrier space (here \mathbb{Z}_n). Due to $(n-1) \oplus 1 = 0$, the \oplus -operation describes iteration over a periodically repeating or cyclic space. This is responsible for some of the beneficial structural properties of the operators in the Hilbert space

$$\mathcal{H}_n := \mathcal{H}(\mathbb{Z}_n, \mathbb{C}). \quad (9)$$

Instead of considering the elements of \mathcal{H}_n as arbitrary functions on the finite space \mathbb{Z}_n one may likewise consider them as periodic functions of period n on the infinite space \mathbb{Z} . Instead of letting the function values be complex numbers one could let them be pairs of real numbers and hide the machinery of complex arithmetics behind a formalism

⁴see [1] for a discussion of subsystems in quantum mechanics

⁵It is an interesting question, however, to what extend one may replace the finite set of computer numbers by a true finite field as advocated by many authors, e.g. [2], or even by a finite ring — which would be sufficient for the direct midpoint integrator, as it needs no division.

of real two by two matrices just as Dirac's complex-valued gamma matrices hide the machinery of quaternion arithmetics.

A natural self-adjoint operator is the *discrete position operator* X given by

$$(X\psi)_i := i\psi_i \text{ for all } \psi \in \mathcal{H}_n, i \in \mathbb{Z}_n, \quad (10)$$

where multiplying the complex number ψ_i with $i \in \mathbb{Z}_n$ ⁶ is well defined by understanding $\mathbb{Z}_n \subset \mathbb{Z} \subset \mathbb{R} \subset \mathbb{C}$. More general, we associate with any function $f : \mathbb{Z} \rightarrow \mathbb{C}$ the linear operator $f(X)$ by

$$(f(X)\psi)_i := f(i)\psi_i \text{ for all } \psi \in \mathcal{H}_n, i \in \mathbb{Z}_n. \quad (11)$$

All operators of this kind commute with each other: $f_1(X)f_2(X) = f_2(X)f_1(X)$, and each linear operator that commutes with X is of this kind. If f is real-valued, as in (10), this operator is self-adjoint since $f(X)^* = \overline{f}(X)$. The discrete position operator (10) is not the only one that suggests itself. Actually, for each $s \in \mathbb{Z}$ the operator X_s defined as

$$(X_s\psi)_i := (i \oplus s)\psi_i \text{ for all } \psi \in \mathcal{H}_n, i \in \mathbb{Z}_n \quad (12)$$

is a discrete position operator for a different choice of the origin. One easily finds a function f for which $X_s = f(X)$.

Now we consider induced operators which are in a sense complementary to the multiplication operators considered so far. For each $s \in \mathbb{Z}$, we define the *translation operator* T_s by

$$(T_s\psi)_i := \psi_{i \oplus s} \text{ for all } \psi \in \mathcal{H}_n, i \in \mathbb{Z}_n. \quad (13)$$

which gives rise to the following canonical properties (for all $s, t \in \mathbb{Z}$)

$$T_s T_t = T_{s+t}, \quad T_s^* = T_{-s} = T_s^{-1}, \quad T_0 = \mathbf{1}, \quad T_s X_t = X_{t+s} T_s. \quad (14)$$

The last equation of (14) is a version of the Heisenberg commutation relations which fits the present framework. Further, we define the *reflection operator* R by

$$(R\psi)_i := \psi_{\rho(i)} \text{ for all } \psi \in \mathcal{H}_n, i \in \mathbb{Z}_n. \quad (15)$$

which satisfies for all $s \in \mathbb{Z}$

$$T_s R = R T_{-s}, \quad R^2 = \mathbf{1}, \quad R^* = R = R^{-1}. \quad (16)$$

Simple combinations of the translation operators define *discrete derivation operators*

$$\nabla_+ := T_1 - T_0, \quad \nabla_- := T_0 - T_{-1}, \quad \nabla := \frac{1}{2}(\nabla_+ + \nabla_-), \quad (17)$$

which satisfy

$$\nabla_+^* = -\nabla_-, \quad \nabla_-^* = -\nabla_+, \quad \nabla^* = -\nabla, \quad R\nabla = -\nabla R, \quad (18)$$

⁶unlike the imaginary unit, which is always written as i (i.e. not in italics)

and that the *discrete Laplacian*

$$\Delta := T_1 - 2T_0 + T_{-1}, \quad (19)$$

which satisfies

$$\Delta = \nabla_+ \nabla_- = \nabla_- \nabla_+, \quad \Delta^* = \Delta, \quad R\Delta = \Delta R. \quad (20)$$

The discrete Laplacian plays a distinguished role in the present framework since we use negative multiples of it as Hamilton operator for free motion of particles. Understanding the eigenvalues of this operator will help in Section 5. Specializing the definition (1) we consider the function Q_Δ . For all $\psi \in \mathcal{H}$, $\|\psi\| = 1$, we have

$$Q_\Delta(\psi) = \langle \psi | \Delta \psi \rangle = \langle \nabla_-^* \psi | \nabla_+ \psi \rangle = -\langle \nabla_+ \psi | \nabla_+ \psi \rangle = -\|\nabla_+ \psi\|^2 \leq 0, \quad (21)$$

which implies that all eigenvalues of Δ are less or equal zero. Obviously, each constant state (i.e. ψ_i independent of i) is eigenvector for eigenvalue 0, so that we have established that 0 is the largest eigenvalue of Δ . It is clear from the definition of Δ that minimizing $Q_\Delta(\psi)$ means for ψ to deviate from constancy as much as possible. An obvious behavior of this kind is what sometimes is called a variation at spatial *Nyquist frequency*. This gives rise to what one may call *Nyquist state*:

$$v_i = \frac{1}{\sqrt{n}} (-1)^i. \quad (22)$$

It is easily seen to satisfy

$$(\nabla_+ v)_i = \begin{cases} -2v_i & \text{if } 0 \leq i < n-1 \\ -2v_i & \text{if } i = n-1 \text{ and } n \text{ is even} \\ 0 & \text{if } i = n-1 \text{ and } n \text{ is odd} \end{cases}, \quad (23)$$

which implies with (21)

$$\langle v | \Delta v \rangle = -4 \cdot \begin{cases} 1 & \text{if } n \text{ is even} \\ 1 - \frac{1}{n} & \text{else} \end{cases}. \quad (24)$$

We see, that for odd n the Nyquist state is not likely to minimize Q_Δ exactly, since the first and the last component being equal in this case, the state does not everywhere vary at maximum frequency. The larger n , the less important is this admixture of a lower frequency. If n is even, in generalization of what (23) says for this case, v is eigenvector for all relevant operators

$$\nabla_+ v = -2v, \quad \nabla_- v = 2v, \quad \Delta v = -4v. \quad (25)$$

This makes the following very plausible: The eigenvalues of Δ lie in the interval $[-4, 0]$, where 0 is always an eigenvector and -4 only if n is even. If n is odd, the lowest eigenvalue is very close to -4 . Numerical results completely agree with this. For instance, for $n = 200$ the lowest five eigenvalues⁷ are

$$-3.996053457, \quad -3.996053457, \quad -3.999013121, \quad -3.999013121, \quad -4.000000000$$

⁷computation of all 200 eigenvalues and eigenvectors took 8.422 s on an off-the-shelf 2.08 GHz desktop computer with my code based on functions *tred2* and *tqli* of [6]

and for $n = 201$ these are

$$-3.993895830, \quad -3.997801783, \quad -3.997801783, \quad -3.999755714, \quad -3.999755714.$$

In the following I describe the basic features of spectral decompositions of Δ as seen in numerous numerical examples. Eigenvalue 0 has always multiplicity 1, and the corresponding eigenvector is and constant and, hence, even. *Even* and *odd states* are, by definition, eigenvectors of the two projectors

$$P_{\text{even}} = \frac{1}{2}(\mathbf{1} + R), \quad P_{\text{odd}} = \frac{1}{2}(\mathbf{1} - R), \quad (26)$$

which, according to (20), commute with Δ . If n is even, the lowest eigenvalue is -4 and has multiplicity 1. The corresponding eigenvector is odd and is a multiple of the Nyquist state. If n is odd, the lowest eigenvalue is slightly larger than -4 and has multiplicity 2. The components of these eigenvectors change sign from i to $i + 1$ just as the Nyquist state but the absolute value of these components varies slowly with i . For large n , the distance between adjacent eigenvalues shrinks strongly towards both ends of the spectrum, so that the lowest eigenvalue has a very close neighbor. It makes thus little difference whether the lowest eigenvalue has multiplicity 1 or 2. All eigenvalues between of the lowest and the highest have multiplicity 2 and can be selected as an odd state and an even state. For the norm $\|\Delta\|$ only the absolute values of the eigenvalues matter, so the conclusion of our discussion

$$\|\Delta\| = 4 \text{ for } n \text{ even, and } \|\Delta\| \approx 4 \text{ for } n \text{ odd.} \quad (27)$$

We observe in passing that none of these operators was defined as a matrix. The representation of linear operators as matrices is not more natural in the finite-dimensional situation than it is in the infinite-dimensional one. Treating \mathcal{H}_n as a function space (with discrete argument) is more natural in most situations. In the computational part of this article we will never have to consider matrices, still less spectral decomposition of matrices. This is important for practical applicability: A reasonable discretization of one spatial direction asks for something like 100 discrete points. Therefore, 1-dimensional quantum simulations would have to cope with complex 100 by 100 matrices. This is no problem, since to compute eigenvalues and eigenvectors of such matrices is a matter of seconds on modern off-the-shelf desktop computers (see footnote 7). However, doing this for a 2-dimensional problem would involve 10000 by 10000 matrices which is hardly feasible.

3 Defining the direct midpoint integrator

Actually we will consider the integrator defined in equation (86) of [4] for the simplifying situation that the Hamiltonian does not depend on time.

Since the method comes from classical mechanics, we start with describing it for the simplest pertinent situation — the initial value problem for a classical mass point

moving in a force field. We write the equation of motion as

$$m\ddot{x} = F(x) \quad (28)$$

and the initial values as $x(0)$ and $v(0)$, where $v := \dot{x}$. We want to compute the system state $x(h), v(h)$ after a time step of duration h . The Euler method does this as follows:

$$a := F(x(0))/m, \quad x(h) := x(0) + hv(0) + \frac{h^2}{2}a, \quad v(h) := v(0) + ha. \quad (29)$$

Here, the formula for $x(h)$ can be given a more economic form, which assumes that v was computed first

$$x(h) = x(0) + \frac{h}{2}(v(h) + v(0)). \quad (30)$$

The well-known practical failure of this method seems to have convinced a majority of scientists that the situation asks more for mathematical sophistication than for physics-based intuition. For instance, implicit versions of the Euler method have been devised, which gain a lot from the viewpoint of numerical mathematics but completely lose the physical plausibility of the original⁸. The *direct midpoint method* [3], [4], [5] is as simple and as plausible as the Euler method. It enjoys the worthy properties of being reversible and symplectic. And it is second order, whereas the Euler method is only first order. The definition is as follows:

$$x' := x(0) + \frac{h}{2}v(0), \quad a := F(x')/m, \quad x(h) := x(0) + hv(0) + \frac{h^2}{2}a, \quad v(h) := v(0) + ha, \quad (31)$$

where the formula for $x(h)$ can also be written as

$$x(h) = x' + \frac{h}{2}v(h). \quad (32)$$

Here one natural idea has been added to the Euler procedure: Since we are going to approximate the system path by a parabola, we should use a value for the constant acceleration a which reasonably can replace the drifting acceleration values of the true motion during the time span of duration h . Obviously, the midpoint in time, $\frac{h}{2}$, would be the most natural time point for the computation of a . Since we don't know $x(\frac{h}{2})$ for a definition $a := F(x(\frac{h}{2}))$, we use the directly available $x(0) + \frac{h}{2}v(0)$ instead. This is a natural strategy to employ the available information.

To motivate the application to quantum mechanics, it may be instructive to follow my own way, which was to use it first for classical continuum mechanics. Let us again look for the simplest pertinent problem, which is the initial value problem for the wave equation in one spatial dimension. Here we have for uniformly discretized space and in suitable units the equation

$$\ddot{\Psi}_i = \Psi_{i-1} - 2\Psi_i + \Psi_{i+1}, \quad (33)$$

⁸ building on Einstein's famous dictum that God does not throw dice, I am tempted to conjecture that He does not solve equations either

and the initial values $\psi_i(0)$ and $\phi_i(0)$, where $\phi_i := \psi'_i$. The definition

$$\begin{aligned}\psi'_i &:= \psi_i(0) + \frac{h}{2}\phi_i(0), & \alpha_i &:= \psi'_{i-1} - 2\psi'_i + \psi'_{i+1}, \\ \phi_i(h) &:= \phi_i(0) + h\alpha_i, & \psi_i(h) &:= \psi'_i + \frac{h}{2}\phi_i(h)\end{aligned}\tag{34}$$

turned out to simulate traveling waves without detectable tendency to change shape or to increase the amplitude. What is different for the Schroedinger equation of a free particle in the same discrete space? Also here, we get an equation for the second time derivative of the wave function by applying the Hamilton operator twice. For a free particle this results in the equation for bending waves in elastic substrates (a rod in one dimension and a plate in two dimensions). The essential difference of the Schroedinger wave compared to such a classical bending wave is in the role of the velocity. For the Schroedinger wave this cannot be set arbitrarily as an initial condition but is prescribed by the Schroedinger equation⁹ as a function of the state ψ

$$\dot{\psi} = -iH\psi.\tag{35}$$

From a computational point of view this makes no difference. We are free to set the initial velocity by (35) and then follow the evolution of states with a rule for computing the second time derivative just as explained above for the wave equation.

Let us give this strategy a precise form: We define the skew-adjoint operator

$$D := -iH.\tag{36}$$

With the state $\psi \in \mathcal{H}$ we associate a *dynamical state* (ψ, ϕ) , where $\phi := D\psi$ for the initial value of a time-discrete trajectory. The continuation of the trajectory is defined by the general evolution step

$$t \mapsto t+h, \quad (\psi, \phi) \mapsto (\underline{\psi}, \underline{\phi}).^{10}\tag{37}$$

According to the quantum mechanical *direct midpoint integrator* this step is defined as

$$\begin{aligned}\psi' &:= \psi + \frac{h}{2}\phi \\ \alpha &:= D^2\psi' \\ \underline{\phi} &:= \phi + h\alpha \\ \underline{\psi} &:= \psi' + \frac{h}{2}\underline{\phi}.\end{aligned}\tag{38}$$

As in (31) there is a more explicit representation of the final state as

$$\underline{\psi} = \psi + h\phi + \frac{h^2}{2}\alpha.\tag{39}$$

⁹ we assume physical units to be chosen for which $\hbar = 1$

¹⁰ Building such a trajectory by computation is what is called *simulation* in this article.

which suggests an interpretation in which h is replaced by a parameter that varies from 0 to h and thus connects the states ψ and $\underline{\psi}$ by a parabolic curve (in Hilbert space) and the quantities ϕ and $\underline{\phi}$ by a linear curve. Then, everywhere along this connecting curve, ϕ is the time derivative of ψ . If we consider this connecting parabola¹¹ as a *Bézier curve* it determines a *control point* which easily can be recognized as the direct midpoint ψ' . In this way, the inherently time-discrete method contains its own time-continuous representation. This time continuous representation is by mere interpolation; if one needs true detail about the history between ψ and $\underline{\psi}$ one has to reduce the time step in the simulation. The parabolas of adjacent evolution steps fit together in a differentiable manner, even if the time step h changes from one evolution step to the next. Therefore, a sequence of evolution steps gives rise to a quadratic *Bézier spline* as a differentiable representation of the discrete trajectory. Everywhere along this curve, the quantity ϕ equals the time-derivative of ψ . This fully legitimates the name *velocity* for the quantity ϕ . The spurious extra-information contained in the small difference between the two velocity-like quantities ϕ and $D\psi$ allows the time stepping algorithm to achieve tasks (such as exact reversal of trajectories) that would be impossible without it. This is a typical example of what computer scientists know as *interplay of data structures and algorithms*.

One could try to avoid to apply the Hamiltonian twice and make use of the direct midpoint state for updating the velocity instead of the acceleration. This leads to the scheme

$$\begin{aligned}\psi' &:= \psi + \frac{h}{2} \phi \\ \underline{\phi} &:= D\psi' \\ \underline{\psi} &:= \psi + h\underline{\phi}\end{aligned}\tag{40}$$

which, however, is definitely inferior to the first method in all respects that I considered, except of the obvious one that it is a bit simpler. So it will not be discussed further.

4 Properties of the direct midpoint integrator

For this section, let \mathcal{H} be any complex Hilbert space of finite dimension d (n will be needed for a different purpose), D any skew-adjoint linear operator in \mathcal{H} , and $H := iD$. Although most comments will refer to the situation that H is the Hamilton operator¹² in a computational model of a quantum system, this interpretation adds nothing that is required for the mathematics to work.

The form (38) of the evolution algorithm aims at minimizing the computational work needed to produce a time-discrete trajectory. Structural properties of the evolution al-

¹¹ here we exclude the trivial case $\alpha = 0$ for which this is actually a straight line

¹² Considering the discrete derivation operator ∇ of (17) as D is also interesting. Here we gain the capability of shifting states by fractions of the discretization length in a way that for integer shifts we approximate the translation operators of (13). Defining fractional shifts of discretely defined functions amounts to defining interpolation.

gorithm can better be derived from a reformulation which we consider now: Replacing the direct midpoint state $\underline{\psi}'$ and the acceleration α by their definitions we find

$$\begin{aligned}\underline{\psi} &= \psi + h\phi + \frac{h^2}{2}D^2\psi + \frac{h^3}{4}D^2\phi, \\ \underline{\phi} &= \phi + hD^2\psi + \frac{h^2}{2}D^2\phi.\end{aligned}$$

It suggests itself to turn this into the definition of a linear operator U_h in the Hilbert space $\mathcal{H} \oplus \mathcal{H}$ of dynamical states. Of course, the latter is $\mathcal{H} \times \mathcal{H}$ as a set and is endowed with the scalar product

$$\langle (\psi_1, \phi_1) | (\psi_2, \phi_2) \rangle := \langle \psi_1 | \psi_2 \rangle + \langle \phi_1 | \phi_2 \rangle.$$

and with the natural \mathbb{C} -linear structure. Hence the definition of U_h is

$$\begin{aligned}U_h &: \mathcal{H} \oplus \mathcal{H} \rightarrow \mathcal{H} \oplus \mathcal{H}, \\ U_h(\psi, \phi) &:= \left(\psi + h\phi + \frac{h^2}{2}D^2\psi + \frac{h^3}{4}D^2\phi, \phi + hD^2\psi + \frac{h^2}{2}D^2\phi \right).\end{aligned}\tag{41}$$

Notice that here — by the very nature of $\mathcal{H} \times \mathcal{H}$ — no relation between ψ and ϕ is assumed. Each linear operator A in $\mathcal{H} \oplus \mathcal{H}$ determines a matrix $\begin{pmatrix} A_{11} & A_{12} \\ A_{21} & A_{22} \end{pmatrix}$ of linear operators in \mathcal{H} such that

$$A(\psi, \phi) = (A_{11}\psi + A_{12}\phi, A_{21}\psi + A_{22}\phi)\tag{42}$$

and each such matrix of operators determines a linear operator in $\mathcal{H} \oplus \mathcal{H}$ through this formula. If the space under consideration is clear from the context, it is allowed to write the zero-operator as 0 and the unit-operator as 1. The operator determined by a matrix $\begin{pmatrix} B & 0 \\ 0 & C \end{pmatrix}$ it is usually written as $B \oplus C$. This notation allows us to write

$$U_h = \begin{pmatrix} 1 - \frac{h^2}{2}H^2 & h(1 - \frac{h^2}{4}H^2) \\ -hH^2 & 1 - \frac{h^2}{2}H^2 \end{pmatrix}.\tag{43}$$

Since all powers H^n of H are defined on our finite-dimensional \mathcal{H} , all powers

$$U_h^n := (U_h)^n$$

are well defined too. We thus have a linear dynamical system, which depends on the step duration h as a parameter.

Even for the physically trivial case that H is the zero-operator, U_h is not completely trivial; it is simple enough that one can write down U_h^n :

$$U_h^n = \begin{pmatrix} 1 & nh \\ 0 & 1 \end{pmatrix}.\tag{44}$$

Applying this to a vector gives

$$U_h^n \begin{pmatrix} \Psi \\ \phi \end{pmatrix} = \begin{pmatrix} \Psi + nh\phi \\ \phi \end{pmatrix}, \quad (45)$$

which corresponds to a motion with constant velocity ϕ . This reduces to trivial dynamics if ϕ is set according to the Schrodinger equation as $\phi = -iH\psi = 0$. Obviously, the matrix in (44) is neither unitary nor normal (unless $nh = 0$) and this will hold for the general case all the more. The simple example $H = 0$ shows that this is not a technical deficiency but a rather natural situation for the dynamical scheme under consideration.

We start our investigation with the properties that do not need an explicit representation of U_h^n in terms of a spectral decomposition of H .

4.1 Invariance under motion reversal

A short calculation involving several potentially surprising cancellations yields

$$U_h U_{-h} = 1 \text{ for all } h \in \mathbb{R} \quad (46)$$

and, as a direct consequence,

$$U_h^n U_{-h}^n = 1 \text{ for all } h \in \mathbb{R}, n \in \mathbb{N}. \quad (47)$$

This implies that each operator U_h^n is invertible, with an inverse that can be given explicitly. The operators U_h^n and U_{-h}^n can be transformed into each other by the simple unitary operator

$$T : \mathcal{H} \oplus \mathcal{H} \rightarrow \mathcal{H} \oplus \mathcal{H}, \quad T(\psi, \phi) := (\psi, -\phi), \quad (48)$$

which obviously satisfies

$$T^2 = 1, \quad T U_h^n = U_{-h}^n T \text{ for all } h \in \mathbb{R}, n \in \mathbb{N}. \quad (49)$$

This implies

$$T U_h^n T U_h^n = 1 \text{ for all } h \in \mathbb{R}, n \in \mathbb{N}, \quad (50)$$

so that one can reconstruct any (ψ, ϕ) from the result $U_h^n(\psi, \phi)$ of a long simulation run (i.e. large n) by applying T on this state and subjecting this transformed state again to n steps of normal dynamical evolution (not one with negative h) and finally applying operator T again. This is exact mathematically and deviations from it in computer simulations are only due to numerical noise. It should be recognized that no anti-linear operator is needed to achieve this reversal of motion in the present dynamical scheme. This is, of course, due to the fact that we have available the velocity ϕ , the reversal of which causes the desired effect just as the reversal of particle velocities achieves motion reversal in classical mechanics.

4.2 Explicit representation

It certainly helps to understand the most simple case, which happens if \mathcal{H} is one-dimensional. Then it is no restriction of generality to interpret \mathcal{H} as \mathbb{C} , and H as a real number. We then read the right-hand side of equation (43) as a real two by two matrix to get a definition of U_h for this concrete case. One computes the n -th power of this matrix by diagonalization:

$$U_h^n = \begin{pmatrix} Q & -Q \\ 1 & 1 \end{pmatrix} \begin{pmatrix} \lambda_1^n & 0 \\ 0 & \lambda_2^n \end{pmatrix} \frac{1}{2} \begin{pmatrix} 1/Q & 1 \\ -1/Q & 1 \end{pmatrix}, \quad \text{where} \\ Q := \frac{\sqrt{h^2 H^2 - 4}}{2H} \quad \text{and} \\ \lambda_{1,2} := 1 - \frac{h^2 H^2}{2} \mp \frac{hH}{2} \sqrt{h^2 H^2 - 4}. \quad (51)$$

Obviously $\lambda_1 \lambda_2 = 1$. For $|hH| < 2$ we get intermediary complex expressions for a real final result, and also in the case $|hH| > 2$, where everything is real, one can transform the terms such that the dependence on n becomes more transparent. A straightforward calculation gives

$$U_h^n = \begin{pmatrix} \cos(nh\hat{B}) & \frac{\hat{A}}{H} \sin(nh\hat{B}) \\ -\frac{H}{\hat{A}} \sin(nh\hat{B}) & \cos(nh\hat{B}) \end{pmatrix}, \quad \lambda_{1,2} = \exp(\mp i h \hat{B}), \quad \text{where} \\ \hat{A} := \sqrt{1 - \frac{h^2}{4} H^2}, \\ \hat{B} := \frac{2}{h} \arctan \frac{hH}{2\hat{A}} = H \left(1 + \frac{1}{24} h^2 H^2 + \frac{3}{640} h^4 H^4 \right) + O(h^6) \quad (52)$$

in the first case, and

$$U_h^n = (-1)^n \begin{pmatrix} \cosh(nh\tilde{B}) & \frac{\tilde{A}}{H} \sinh(nh\tilde{B}) \\ \frac{H}{\tilde{A}} \sinh(nh\tilde{B}) & \cosh(nh\tilde{B}) \end{pmatrix}, \quad \lambda_{1,2} = -\exp(\pm h\tilde{B}), \quad \text{where} \\ \tilde{A} := \sqrt{\frac{h^2}{4} H^2 - 1}, \\ \tilde{B} := \frac{1}{h} \log \left(hH\tilde{A} + \frac{h^2 H^2}{2} - 1 \right), \quad (53)$$

in the second case, and finally

$$U_h^n = (-1)^n \begin{pmatrix} 1 & 0 \\ nhH^2 & 1 \end{pmatrix}, \quad \lambda_{1,2} = -1, \quad (54)$$

for the degenerate case $|hH| = 2$. In the first case, there is a bound for $\|U_h^n\|$ which is independent of n , whereas in the second case $\|U_h^n\|$ grows exponentially with n . It is natural to refer to these three cases as *stable*, *unstable*, and *indifferent*.

Let us now return to the general case in which \mathcal{H} is d -dimensional. To reduce this case to (52), (53), (54) we choose a spectral decomposition $(e_i)_{i=1}^d, (\varepsilon_i)_{i=1}^d$ of H where the indexing is done such that $i < j \Rightarrow |\varepsilon_i| \leq |\varepsilon_j|$. For all $i \in I := \{1, \dots, d\}$ the projector $\mathbf{P}_i := |e_i\rangle\langle e_i|$ commutes with H and the projector $P_i := \mathbf{P}_i \oplus \mathbf{P}_i$ commutes with U_h , and, hence, with U_h^n . Therefore, the 2-dimensional subspace $\mathcal{H}_i := P_i(\mathcal{H} \oplus \mathcal{H})$ is invariant under U_h . The restriction of U_h^n to \mathcal{H}_i , when written as a complex two by two matrix, is given by (51) with H replaced by ε_i . The h -dependent partition $I = \hat{I}_h \cup \tilde{I}_h \cup \bar{I}_h$ with

$$\hat{I}_h := \{i \in I : |\varepsilon_i h| < 2\}, \quad \tilde{I}_h := \{i \in I : |\varepsilon_i h| > 2\}, \quad \bar{I}_h := \{i \in I : |\varepsilon_i h| = 2\}, \quad (55)$$

decides whether for $i \in I$ this complex two by two matrix equals the matrix in (52), or (53), or (54), again with H replaced by ε_i . The projectors

$$\hat{\mathbf{P}}_h := \sum_{i \in \hat{I}_h} \mathbf{P}_i, \quad \tilde{\mathbf{P}}_h := \sum_{i \in \tilde{I}_h} \mathbf{P}_i, \quad \bar{\mathbf{P}}_h := \sum_{i \in \bar{I}_h} \mathbf{P}_i, \quad (56)$$

unveil their origin by satisfying the inequalities

$$\|hH\hat{\mathbf{P}}_h\psi\| < 2\|\hat{\mathbf{P}}_h\psi\|, \quad \|hH\tilde{\mathbf{P}}_h\psi\| > 2\|\tilde{\mathbf{P}}_h\psi\|, \quad \|hH\bar{\mathbf{P}}_h\psi\| = 2\|\bar{\mathbf{P}}_h\psi\| \quad (57)$$

for all $\psi \in \mathcal{H}$. The augmented projectors

$$\hat{\mathbf{P}}_h := \hat{\mathbf{P}}_h \oplus \hat{\mathbf{P}}_h, \quad \tilde{\mathbf{P}}_h := \tilde{\mathbf{P}}_h \oplus \tilde{\mathbf{P}}_h, \quad \bar{\mathbf{P}}_h := \bar{\mathbf{P}}_h \oplus \bar{\mathbf{P}}_h, \quad (58)$$

allow to decompose the space $\mathcal{H} \oplus \mathcal{H}$ into subspaces on which U_h^n is uniform with respect to the property of being stable, unstable, or indifferent. Of course, the projectors in (58) commute with U_h^n , and with each other, and add up to the unit-operator. Therefore, the restriction of U_h^n to the invariant subspace $\hat{\mathbf{P}}_h(\mathcal{H} \oplus \mathcal{H})$ is the expression for U_h^n as given in (52) with H interpreted again as an operator in \mathcal{H} instead of a real number. Corresponding statements hold for the invariant subspaces $\tilde{\mathbf{P}}_h(\mathcal{H} \oplus \mathcal{H})$ and $\bar{\mathbf{P}}_h(\mathcal{H} \oplus \mathcal{H})$. We thus have the following *explicit representation* of U_h^n :

$$U_h^n = \hat{U}_h^n \hat{\mathbf{P}}_h + \tilde{U}_h^n \tilde{\mathbf{P}}_h + \bar{U}_h^n \bar{\mathbf{P}}_h, \quad (59)$$

where \hat{U}_h^n is the expression as given in (52) for U_h^n with H interpreted an operator in \mathcal{H} . In the same manner \tilde{U}_h^n is understood to originate from (53), and \bar{U}_h^n from (54). All functions of H appearing in these expressions are primarily defined via spectral decomposition of H , just as they originated here. They may be defined also by inserting operators into the power series expansions of the corresponding numerical functions.

According to our ordering of the eigenvalues the set \hat{I}_h grows monotone to I as $|h|$ tends to zero, and $\tilde{I}_h \cup \bar{I}_h$ shrinks monotone to the void set. Whenever

$$|h| < \frac{2}{\|H\|} \quad (60)$$

or $\|H\| = 0$ we have $\hat{I}_h = I$ and thus $\hat{\mathbf{P}}_h = 1$. Then only the first term in (59) is present.

We are now interested in the behavior of U_h^n for small h , especially in $\lim_{n \rightarrow \infty} U_{t/n}^n$ and thus rightfully assume (60). Expansions in powers of h of the quantities \hat{A} and \hat{B} unveils the behavior of U_h^n near the limit. \hat{B} gives rise to the expansion

$$\hat{B} = H \left(1 + \frac{1}{24} h^2 H^2 + \frac{3}{640} h^4 H^4 + \frac{5}{7168} h^6 H^6 + \frac{35}{294912} h^8 H^8 + \dots \right) =: \hat{H}(h), \quad (61)$$

and quantities \hat{A} and $\frac{1}{\hat{A}}$ expand as follows:

$$\begin{aligned} \hat{A}_1(h) &= 1 - \frac{1}{8} h^2 H^2 - \frac{1}{128} h^4 H^4 - \dots, \\ \hat{A}_2(h) &= 1 + \frac{1}{8} h^2 H^2 + \frac{3}{128} h^4 H^4 + \dots. \end{aligned} \quad (62)$$

Equation (59) then implies

$$U_h^n = \begin{pmatrix} \cos(nh\hat{H}(h)) & \frac{1}{H}\hat{A}_1(h) \sin(nh\hat{H}(h)) \\ -H\hat{A}_2(h) \sin(nh\hat{H}(h)) & \cos(nh\hat{H}(h)) \end{pmatrix}. \quad (63)$$

Since $\hat{H}(0) = H$, $\hat{A}_1(0) = \hat{A}_2(0) = 1$, we have

$$\lim_{n \rightarrow \infty} U_{t/n}^n = \begin{pmatrix} \cos tH & \frac{1}{H} \sin tH \\ -H \sin tH & \cos tH \end{pmatrix} =: U_t^\infty, \quad (64)$$

and after some calculation

$$\lim_{n \rightarrow \infty} \left(U_{t/n}^n - U_t^\infty \right) n^2 = -\frac{t^3 H^3}{24} \begin{pmatrix} \sin tH & \frac{1}{H} (3 \frac{\sin tH}{tH} - \cos tH) \\ H (3 \frac{\sin tH}{tH} + \cos tH) & \sin tH \end{pmatrix}. \quad (65)$$

Applying operator (63) to an initial dynamical state and re-building the exponential function from the trigonometric functions gives

$$U_h^n \begin{pmatrix} \Psi \\ -iH\Psi \end{pmatrix} = \begin{pmatrix} \exp(-inh\hat{H}(h))\Psi + i\hat{A}_3(h) \sin(nh\hat{H}(h))\Psi \\ -iH(\exp(-inh\hat{H}(h)) - i\hat{A}_4(h) \sin(nh\hat{H}(h)))\Psi \end{pmatrix}, \quad (66)$$

where

$$\begin{aligned} \hat{A}_3(h) &= \frac{1}{8} h^2 H^2 + \frac{1}{128} h^4 H^4 + \dots, \\ \hat{A}_4(h) &= \frac{1}{8} h^2 H^2 + \frac{3}{128} h^4 H^4 + \dots \end{aligned} \quad (67)$$

are the expansions of $1 - \hat{A}$ and $\frac{1-\hat{A}}{\hat{A}}$. Therefore, or directly from (64),

$$\lim_{n \rightarrow \infty} U_{t/n}^n \begin{pmatrix} \Psi \\ -iH\Psi \end{pmatrix} = \begin{pmatrix} \exp(-itH)\Psi \\ -iH \exp(-itH)\Psi \end{pmatrix}. \quad (68)$$

To understand the effect of replacing the exact dynamics (68) by (66), we assume that Ψ is an eigenvector of H with eigenvalue ε . Further, we consider only the state

component and not the velocity. The main effect is that the dynamical phase factor $\exp(-i t \varepsilon)$ gets replaced by $\exp(-i t \varepsilon(1 + \frac{1}{24} h^2 \varepsilon^2))$ and that the term $-i \frac{1}{8} h^2 \varepsilon^2 \sin(t \varepsilon(1 + \frac{1}{24} h^2 \varepsilon^2)) \psi$ gets added to the state. Notice that the whole analysis assumes $h^2 \varepsilon^2 < 4$. Here we see that this is not sufficient to make these modifications small enough for neglecting them in all but the crudest studies. However, if one reduces h to a tenth of the value which just satisfies to the previous condition, the amplitude-changing additive term may be ignorable in most applications. The frequency shift is still large enough that the simulated wave runs out of phase by a full period after 600 oscillations.

In a sense, the Hamiltonian H acts as an renormalized Hamiltonian $H(1 + \frac{1}{24} h^2 H^2)$. Replacing the original Hamiltonian by $H(1 - \frac{1}{24} h^2 H^2)$ would let the new renormalized Hamiltonian come close to the original H . In a realistic time-discrete model of a quantum system, space is discretized too, and the Hamiltonian (and its eigenvalues) depends on the spatial discretization length. A meaningful assessment of the accuracy with which a discretized system is able to represent a continuous one, needs to take the interplay of both discretizations into account.

4.3 Conservation of energy and semi-conservation of the norm of the initial state

Let us consider the sequence of states resulting from a simulation which starts with state $\psi \in \mathcal{H}$. As pointed out earlier, we put $\phi := -iH\psi$ to arrive at the initial dynamical state (ψ, ϕ) . The computation of the trajectory proceeds by iteration:

$$(\psi_h^1, \phi_h^1) := U_h(\psi, \phi), \quad (\psi_h^{n+1}, \phi_h^{n+1}) := U_h(\psi_h^n, \phi_h^n). \quad (69)$$

Of course,

$$(\psi_h^n, \phi_h^n) = U_h^n(\psi, \phi). \quad (70)$$

It is clear, however, that using U_h^n is not a method for computing a trajectory. If we had a spectral decomposition of H , which underlies the explicit representation of U_h^n , we would compute the exact expression $\exp(-itH)\psi$ directly. However, as we will see, the representation (70) together with (59) is able to explain general properties of trajectories which would not easily be derived from the definition by iteration.

For the exact version $(e^{-inhH}\psi, -iHe^{-inhH}\psi)$ of (ψ_h^n, ϕ_h^n) (see (68)) one would have exact unitarity and exact energy conservation so that the difference quantities

$$v(\psi, n, h) := \langle \psi_h^n | \psi_h^n \rangle - \langle \psi | \psi \rangle, \quad \varepsilon(\psi, n, h) := \langle \psi_h^n | \phi_h^n \rangle - \langle \psi | \phi \rangle \quad (71)$$

relative to the initial state would vanish for all $n \in \mathbb{N}$. Therefore, these quantities are expected to remain small in regular simulations. For having a natural notion of smallness we define the relative quantities

$$v_{\text{rel}}(\psi, n, h) := \frac{v(\psi, n, h)}{\langle \psi | \psi \rangle}, \quad \varepsilon_{\text{rel}}(\psi, n, h) := \frac{\varepsilon(\psi, n, h)}{|\langle \psi | \phi \rangle|}. \quad (72)$$

For the demonstration system of Section 5 these quantities are shown in Figure 7 as functions of model time $t = nh$ for the fixed value h of the simulation. Since computing

these quantities does not add significantly to the computational burden of a simulation, I created corresponding diagrams throughout my development work on quantum simulation. Although the systems varied considerably, all these diagrams showed striking similarities. Actually, it was this observation that let me expect that an explicit analysis of the direct midpoint method for arbitrary Hamiltonians would be feasible. Now, that the representation (59) is established, it is straightforward to deduce these general properties. It might be instructive to state them as observations first, and come to the explanation later on:

- (i) $v_{\text{rel}}(\psi, n, h)$ starts with 0 and drops soon to small negative values and never becomes positive
- (ii) $\Im \varepsilon_{\text{rel}}(\psi, n, h)$ is 0 up to numerical noise
- (iii) The curve $\Re \varepsilon_{\text{rel}}$ looks like being proportional to the derivative of the curve v_{rel}

The shape of these curves with their partly flat, partly wavy, course is not easy to understand at a first glance. The first observation is that the curve shape does not change significantly when the step size h gets changed, as far as the range of the variable nh remains the same. Using auto-scaled graphical representation of v_{rel} and ε_{rel} (or even v and ε) makes this evident. It turns out that doubling the numbers of steps used to cover a span of model time reduces v_{rel} and ε_{rel} to a quarter of their original values. This suggests to consider the quantities

$$v_{\text{scaled}}(\Psi, n, h) := \frac{v(\Psi, n, h)}{h^2}, \quad \varepsilon_{\text{scaled}}(\Psi, n, h) := \frac{\varepsilon(\Psi, n, h)}{h^2} \quad (73)$$

for which the observation is

- (iv) $v_{\text{scaled}}(\Psi, n, h)$ and $\varepsilon_{\text{scaled}}(\Psi, n, h)$ depend on n and h predominantly through their product $t = nh$

In the case of Figures 8, 9 the curves from three runs with h -values related as 1 : 2 : 4 collapse perfectly (within the graphical resolution) to a single curve in agreement with the previous formulation. Not for all run data, the match is as perfect as in the present case. The limiting curve shape, thus is seen to depend only on the initial state, the time interval, and the Hamiltonian, just as the exact time continuous trajectory.

Let us now look for explanations. The representation (59) gives explicit expressions for the quantities in equation (71). To derive these, we decompose ψ by means of projectors (56):

$$\psi = \hat{\mathbf{P}}_h \psi + \tilde{\mathbf{P}}_h \psi + \bar{\mathbf{P}}_h \psi =: \hat{\psi} + \tilde{\psi} + \bar{\psi}. \quad (74)$$

Since the projectors (56) project on mutually orthogonal subspaces, we have

$$v(\psi, n, h) = v(\hat{\psi}, n, h) + v(\tilde{\psi}, n, h) + v(\bar{\psi}, n, h) \quad (75)$$

and

$$\varepsilon(\psi, n, h) = \varepsilon(\hat{\psi}, n, h) + \varepsilon(\tilde{\psi}, n, h) + \varepsilon(\bar{\psi}, n, h). \quad (76)$$

From (52) we have

$$\begin{aligned} v(\hat{\Psi}, n, h) &= -\frac{h^2}{4} \|H \sin(nh\hat{B}) \hat{\Psi}\|^2, \\ \varepsilon(\hat{\Psi}, n, h) &= -\frac{h^2}{8} \langle \hat{\Psi} | \frac{H^3}{A} \sin(2nh\hat{B}) \hat{\Psi} \rangle, \end{aligned} \quad (77)$$

and from (53)

$$\begin{aligned} v(\tilde{\Psi}, n, h) &= \frac{h^2}{4} \|H \sinh(nh\tilde{B}) \tilde{\Psi}\|^2, \\ \varepsilon(\tilde{\Psi}, n, h) &= \frac{h^2}{8} \langle \tilde{\Psi} | \frac{H^3}{A} \sinh(2nh\tilde{B}) \tilde{\Psi} \rangle, \end{aligned} \quad (78)$$

and, finally, from (54)

$$\begin{aligned} v(\bar{\Psi}, n, h) &= 0, \\ \varepsilon(\bar{\Psi}, n, h) &= 4 \frac{n}{h} \langle \bar{\Psi} | \bar{\Psi} \rangle. \end{aligned} \quad (79)$$

Ad (i): Consider the first equation in (78): It says that $\langle \Psi_h^n | \Psi_h^n \rangle$ grows exponentially with n if $\tilde{\mathbf{P}}_h \psi$ does not vanish. This is very likely to be seen in any simulation run in which the step duration h was chosen at random. The present theory assures: Reduction of $|h|$ will finally achieve $\hat{\mathbf{P}}_h \psi = \psi$ and thus $\tilde{\mathbf{P}}_h \psi = 0$ (and $\bar{\mathbf{P}}_h \psi = 0$, deviations from which could happen only intentionally). Then the equations (77) are active with $\hat{\Psi} = \psi$. This then implies that $v(\psi, n, h)$ will never become positive, i.e. the norm of the evolving state will never exceed the norm of the initial state. Even states with extreme spikes and jumps are no exception to this rule. However, exponential growth will let even tiny components $\tilde{\mathbf{P}}_h \psi$ become dominant and explode. The only reliable way to prevent such components from being present in the initial state of a computational model, is to set h such that the state-independent criterion (60) is satisfied. To understand why this is the case, we think of the initial wave function as a sum of a ‘mathematical’ function (obtained by understanding all functions and operations in the sense of mathematics) and a function representing the numerical noise (quantization noise) from the encoding of numbers in terms of a finite number of bits. Due to the linearity of U_h we can consider the fate of these contributions to the initial wave function separately. Whereas the the ‘mathematical’ wave function typically defines an distribution of H -values around $\langle \psi | H \psi \rangle$ with an upper bound of the same order of magnitude, the H -values of the noise wave function will cover the whole possible range, up to the limited $\|H\|$.

In the model of Section 5 the value of $\|H\|$ is determined mainly by the kinetic energy for which the operator norm is known from (27). For making sure that also contributions from the interaction potential are properly taken into account, I devised a semi-empirical algorithm for finding a good estimate for $\|H\|$ directly from H and ψ : The iteration scheme

$$\psi_0 := \psi, \quad \chi := H \psi_i, \quad \eta_i := \|\chi\|, \quad \psi_{i+1} := \frac{1}{\eta_i} \chi \quad (80)$$

yields a sequence (η_1, η_2, \dots) of positive numbers and a sequence (ψ_1, ψ_2, \dots) of states with the following properties: The first few values of η_i correspond to the distribution of energy values determined by the ‘mathematical’ wave function. The η -sequence then grows soon to much higher values near $\|H\|$. Visualizing the corresponding states ψ_i is interesting: as η grows, the states show over increasing areas a uniform checkerboard pattern, which in two dimensions corresponds to the Nyquist state (22). I found it always sufficient to compute at most 100 iterations. This is then no noticeable addition to the computational work of a simulation which typically does thousands of steps. For steps set small enough to prevent numerical noise to grow, the intentional features of the system such as trajectories of centers of wave packets get typically represented with very good accuracy, so that a comparison of one run with a control run with step $h/2$ will essentially indistinguishable results. The same would hold true in most cases for doubling the step if one could execute the algorithm according to exact mathematics. But with computer mathematics one will get explosion, unless h was set overcautious.

Ad (ii): The formulas for ε say that it is real in all cases. Thus $\langle \psi_h^n | \phi_h^n \rangle$ differs from $\langle \psi | \phi \rangle = -i \langle \psi | H \psi \rangle$ by a real quantity. Therefore, $\Im \langle \psi_h^n | \phi_h^n \rangle = -\langle \psi | H \psi \rangle$ and $\Re \langle \psi_h^n | \phi_h^n \rangle = \varepsilon(\psi, n, h)$ for all n . This can be interpreted as exact conservation of energy. It is to be noted, however, that $\langle \psi_h^n | \phi_h^n \rangle$ equals $-i \langle \psi_h^n | H \psi_h^n \rangle$ only approximately, so that it is not really the expectation value of the Hamilton operator which is conserved exactly.

Ad (iii): Since the function v is related to the change of the norm of a state and the function ε is related to an imaginary contribution to the expectation value of the Hamiltonian, one expects that these functions are related. Actually, (52) and (53) imply

$$nh \varepsilon(\psi, n, h) = \left(\frac{h}{2} \frac{d}{dh} - 1 \right) v(\psi, n, h) \quad (81)$$

for all h such that $\bar{P}_h \psi = 0$. I had guessed this equation before, by extrapolating power series results got for U_h^n for $n = 1, 2, \dots, 15$ by means of a computer algebra system. Even with (52) and (53) given, verifying the equation is easier than finding it. The observation (iv) pointed more to a relation between limits rather than to an exact equation between the functions v and ε . Since this relation involves a derivative with respect to h , it connects data from different simulations (differing in h to allow computing the derivative). This lets the equation appear quite cryptic. Two functions which are related approximately by a derivation within a single simulation will appear in (82).

Ad (iv): Making use of (61) one finds

$$\begin{aligned} v_{\text{scaled}}(\hat{\Psi}, n, h) &= -\frac{1}{4} \|H \sin(nh\hat{H}(h)) \hat{\Psi}\|^2 \xrightarrow{h \rightarrow 0} -\frac{1}{4} \|H \sin(nhH) \hat{\Psi}\|^2 =: \tilde{v}(\hat{\Psi}, nh), \\ \varepsilon_{\text{scaled}}(\hat{\Psi}, n, h) &= -\frac{1}{8} \langle \hat{\Psi} | H^3 \sin(2nh\hat{H}(h)) \hat{\Psi} \rangle \xrightarrow{h \rightarrow 0} -\frac{1}{8} \langle \hat{\Psi} | H^3 \sin(2nhH) \hat{\Psi} \rangle =: \tilde{\varepsilon}(\hat{\Psi}, nh). \end{aligned} \quad (82)$$

As a result of this, simulation runs of a system for different values of the time step give nearly identical curves for the quantities v_{scaled} and $\varepsilon_{\text{scaled}}$ if represented as functions

of time $t = nh$ and not simply as a function of the step number. For the scaling limits \tilde{v} and $\tilde{\epsilon}$ one verifies directly $\frac{d}{dt}\tilde{v}(\psi, t) = 2\tilde{\epsilon}(\psi, t)$ which can also be derived from the equation (81) for the unscaled quantities.

The features of the functions \tilde{v} , $\tilde{\epsilon}$ can be understood based on their definition in (82). Employing the same spectral decomposition $(e_i)_{i=1}^d, (\epsilon_i)_{i=1}^d$ of H which was used for the definition of the projector \hat{P}_h , we write for $\psi = \sum_{i=1}^d c_i e_i$

$$\begin{aligned}\tilde{v}(\psi, t) &= -\frac{1}{4} \sum_{i=1}^d |c_i|^2 \epsilon_i^2 \sin^2(t\epsilon_i) = -\frac{1}{8} \sum_{i=1}^d |c_i|^2 \epsilon_i^2 (1 - \cos(2t\epsilon_i)) \\ &= -\frac{1}{8} \|H\psi\|^2 + \frac{1}{8} \sum_{i=1}^d |c_i|^2 \epsilon_i^2 \cos(2t\epsilon_i).\end{aligned}\tag{83}$$

This makes clear, that the curve oscillates around the value $-\frac{1}{8} \|H\psi\|^2$ and attains a first minimum for $2t\epsilon_{\max} \approx \pi$, where ϵ_{\max} is the largest energy value ϵ_i for which $|c_i|$ is significantly larger than 0. In most applications this is much smaller than ϵ_d . Numbers will be discussed in the comments on Figures 8.

5 Simulating the crossway system

Two-dimensional motion of a particle under the influence of potentials has been nicely simulated and visualized by [8]. This is very instructive as an orientation, but it does not unveil the deeper characteristics of quantum dynamics. These can become apparent only in the interaction between quantum systems. Essential for fast computational implementation and visualization of quantum interaction is finding a simple and depictive model of a quantum system involving interaction of subsystems. Here, we will be concerned with systems in which it is motion in space ('real' space, not e. g. a space of spin configurations) which is under the control of interaction.

An obvious choice is a model with two particles, each living in a one-dimensional discrete space as considered in Section 2. If this space is the same for the two particles, one has a peculiar situation: for one particle to move along its space it might have to cross the path of the second particle. If the interaction is strong for short distances, this will cause violent motion which is not common in realistic systems in which particles can move around each other and nevertheless avoid coming under the influence of the strong forces near their centers. Taking this into account, it is a natural idea to arrange the linear biotops of the two particles perpendicular to each other, resembling two crossing roads. Now strong interaction between the particles can be avoided if they don't insist in passing the crossing simultaneously.

We now consider a concrete system. For particle 1 we provide a linear chain of n_1 discrete positions, which we take as the centers x_i of the sub-intervals which result from an interval $[-\frac{L_1}{2}, \frac{L_1}{2}]$ by subdividing it into n_1 congruent parts:

$$x_i = -\frac{L_1}{2} + \left(i + \frac{1}{2}\right) d_1, \quad i \in \{0, \dots, n_1 - 1\} \quad \text{where} \quad d_1 := \frac{L_1}{n_1}.\tag{84}$$

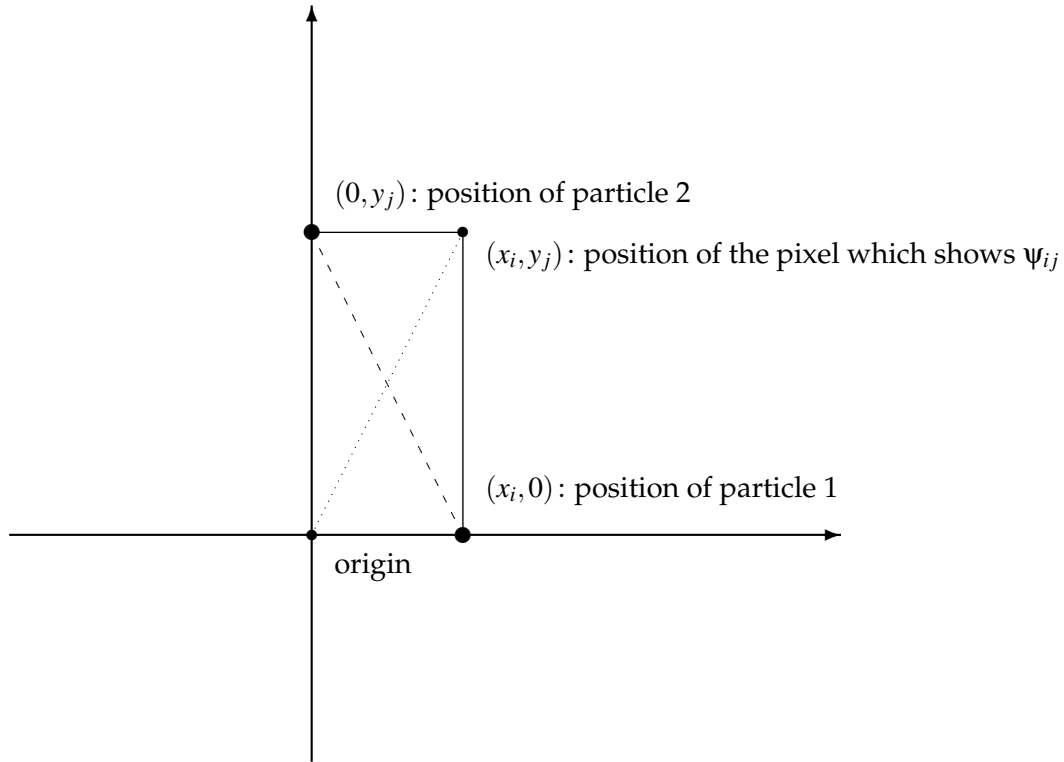


Figure 1: Crossway situation

For particle 2 we imply the same definitions with index 1 replaced by index 2 and with x_i replaced by y_j . Both chains get embedded in an Euclidean plane. Those of particle 1 on the x-axis and those of particle 2 on the y-axis of a Euclidean system of coordinates which we have selected in this plane. The state space of the system consisting of particle 1 and particle 2 is of the form $\mathcal{H}_{n_1} \otimes \mathcal{H}_{n_2}$ consisting of the complex-valued functions on $\mathbb{Z}_{n_1} \times \mathbb{Z}_{n_2}$ and being equipped with the scalar product

$$\langle \Psi | \Phi \rangle := \sum_{i=0}^{n_1-1} \sum_{j=0}^{n_2-1} \bar{\Psi}_{ij} \Phi_{ij}. \quad (85)$$

As indicated already, we interpret ψ_{ij} as the quantum mechanical amplitude associated with the situation that particle 1 is at position x_i of 'street 1' and particle 2 is at position y_j of 'street 2' and thus have the distance

$$r_{ij} := \sqrt{x_i^2 + y_j^2} \quad (86)$$

from each other¹³. (One could associate this amplitude also with the situation that a single particle is at a ‘off-road’ position (x_i, y_j) of the plane and thus has the distance r_{ij} from the origin. Actually, the whole system to be described could be interpreted in this way as a rather artificial 2-dimensional system of a single particle in a potential.) The kinetic part H_0 of the Hamiltonian is of the form $a_1 \Delta \otimes \mathbf{1} + a_2 \mathbf{1} \otimes \Delta$ where the constants a_1, a_2 are expressed in terms of particle masses, lattice spacing, and physical constants as in the following explicit expression

$$(H_0 \Psi)_{ij} := \frac{-\hbar^2}{2m_1 d_1^2} (\Psi_{i-1,j} - 2\Psi_{ij} + \Psi_{i+1,j}) + \frac{-\hbar^2}{2m_2 d_2^2} (\Psi_{i,j-1} - 2\Psi_{ij} + \Psi_{i,j+1}), \quad (87)$$

where $i \pm 1$ is to be understood modulo n_1 , and $j \pm 1$ modulo n_2 . The complete Hamiltonian is $H := H_0 + V$, where

$$(V \Psi)_{ij} := (f_1(x_i) + f_{12}(r_{ij}) + f_2(y_j)) \Psi_{ij}, \quad (88)$$

and f_1, f_{12}, f_2 are suitable functions $\mathbb{R} \rightarrow \mathbb{R}$ for describing interaction with the environment and between the particles. For the system under consideration these functions are as follows:

$$f_1(x) := 0, \quad f_{12}(r) := \alpha \frac{\exp(-\mu r)}{(r + \varepsilon)^{1+p}}, \quad f_2(y) := \beta y^2. \quad (89)$$

For the sake of simplicity this article reports and discusses basically a single computation concerning this system. Of course, in this computation each general parameter has a numerical value, and this value will be added to each such parameter at least once. With this agreement on the parameters, the dynamical system is determined by the following twelve numbers:

- positive integers: $n_1 (= 150), n_2 (= 64)$
- positive reals: $\hbar (= 1), L_1 (= 7.5), L_2 (= 1), m_1 (= 7.5), m_2 (= 8), \varepsilon (= 0.2), \beta (= 308.83)$
- arbitrary reals: $\alpha (= -2.2598), \mu (= 1), p (= 1)$

The classical limit of the system is an interesting two-dimensional dynamical system which resembles the double spring systems presented by P. Lynch in [7]. This offers a good opportunity to compare sets of classical trajectories with the evolution of quantum states. This will, however, not be carried out here.

After having specified the state space and the Hamilton operator, we need to specify the initial state. We choose it as a tensor product state (thus not an entangled one) of a Gaussian wave packet for particle 1 and an eigenstate of the harmonic oscillator Hamiltonian H_2 to which the Hamiltonian (87), (88) reduces for $\alpha = 0$ after re-interpretation as an operator in \mathcal{H}_{n_2} . Let us denote the eigenstates and eigenvalues of H_2 as $\phi_k, \varepsilon_k, k \in \{0, 1, 2, \dots\}$, where the ε_k increase with k .

¹³ If we replace the distance by $r_{ij} := |x_i - y_j|$, we have the case that the two roads coincide rather than cross each other.

The Gaussian state $\psi^1 \in \mathcal{H}_{n_1}$ gets a preliminary definition as

$$\psi_i^1 := \exp\left(-\frac{1}{2}\left(\frac{x_i - x_c}{\sigma}\right)^2\right), \quad (90)$$

where in our case $x_c = -1.5$ and $\sigma = 0.1875$. This is made a normalized state by multiplication with a suitable real constant. This Gaussian bell is sufficiently separated from the boundaries of the biotope (which are at $x = \pm L_1/2, L_1 = 7.5$) that no precautions are needed for making it periodic. (Since the discrete positions 0 and $n_1 - 1$ are neighbors, a large difference between ψ_0 and ψ_{n_1-1} has the same dynamical effect as if this difference would appear somewhere in the interior of the biotope. Such differences can be strongly reduced by replacing the right-hand side term of (90) by a sum of three copies of this term with x_c replaced by $x_c - L_1, x_c, x_c + L_1$ respectively.) This reminds us of the fact that Gaussian wave functions are not canonical in the present context. It could be instructive to imitate in discrete space the analysis which singles out the Gaussian wave functions for quantum mechanics in \mathbb{R} . Due to the good behavior of the naively discretized Gaussians, there seems to be no real need for such an analysis. The wave packet is at rest so far. It gets a velocity v towards the origin (the road crossing) by application of the *boost* operator $N_1(v)$ defined as

$$(N_1(v)\psi)_i := \exp(i v x_i m_1 / \hbar) \psi_i. \quad (91)$$

In our case incidentally $v = 3.14159$. This finishes the definition of the initial state ψ^1 of particle 1.

For particle 2 we choose the ground state ϕ_0 of H_2 . We then have the standard situation of scattering theory: A quantum system in a stable state, the target, gets hit by a projectile, and, as a consequence of this, will evolve into a superposition of stationary states, and also the motion of the projectile will be modified by exchanging energy (and momentum) with the target. Our crossway system will allow to follow this process at the conceptual level of time dependent scattering theory (e.g. [9]), where scattering states are understood as dynamical idealizations of true system trajectories. Actually, the coupling constant β is adjusted such that the kinetic energy of particle 1 (the projectile) equals the energy difference $\epsilon_4 - \epsilon_0$. Eigenvectors and eigenvalues of H_2 are here obtained by the tools mentioned in footnote 7. If one would simply discretize the continuous harmonic oscillator wave functions one would get annoying inaccuracies for low values of n_2 and higher excited states. Notice that the practical convenience of spectral analysis in defining instructive initial conditions does not mean that we need spectral analysis for the definition of the dynamics of our system. Now we define from the state $\psi^1 \in \mathcal{H}_{n_1}$ of particle 1 and the state $\psi^2 \in \mathcal{H}_{n_2}$ of particle 2 (recall $\psi^2 = \phi_0$) the state $\psi := \psi^1 \otimes \psi^2$ of the two-particle system by

$$(\psi^1 \otimes \psi^2)_{ij} := \psi_i^1 \psi_j^2, \quad (92)$$

This state is visualized in Figure 2. The coding of complex numbers as colors is natural: The absolute value controls luminance and the polar angle controls hue. The polar

angle is 0 for red, 120 degrees for green, and 240 degrees for blue. Actually $|\psi_{ij}|^\gamma$ is used to control the luminance with γ set from the control file. Normal values are $\gamma = 0.5$ or $\gamma = 1$. But for inspecting also the areas where the values of the wave function are small and where violations of (60) become visible as expanding checkerboard patterns, much lower values such as $\gamma = 0.01$ are helpful.

The figure shows the whole biotope of the system where the aspect ratio is not conserved and the pixel structure is hidden by interpolation. Recall Figure 1 for the correspondence between graphical position and the positions of the particles in their respective biotops. Since the ground state of the harmonic oscillator is a Gaussian bell too, the initial state is a Gaussian in two dimensions. The colored stripe pattern results from the application of the boost operator. It indicates the velocity of the wave packet, which lets it move towards the center of the frame.

It could be instructive to try a different mode of visualization: Instead of an rectangular image, present a time sequence of graphical events each being of the type: show particle 1 at x_i and particle 2 at y_j both in the same color, namely the one corresponding to the complex number ψ_{ij} . In this form, the method extends naturally to n -particle wave functions in a plane or — making proper use of perspective — even in space. It is not clear however, whether the details can be arranged in a way that the human visual system can convert this graphical process into a useful impression.

5.1 Requirements on the number of discretization points

So far we have set up the concrete version of our system as a computational system in terms of numbers. In order to relate it to an idealized physical system, we have to interpret the numbers as representing physical quantities. The quantities in our system all have dimensions which are clear from the context. Since only mechanical dimensions appear, all physical quantities are defined if a unit \mathbf{L} of length, a unit \mathbf{T} of time, and a unit \mathbf{M} of mass are defined. Setting the numerical value of \hbar in the $(\mathbf{L}, \mathbf{T}, \mathbf{M})$ -system equal to 1 (as we do throughout) means to use units that are related by

$$\mathbf{M} = \frac{\hbar \mathbf{T}}{\mathbf{L}^2}. \quad (93)$$

Let consider particle 1 first. The length $L_1 = 7.5\mathbf{L}$ of the biotope and the number $n_1 = 150$ of discretization points determines a discretization length $d_1 = (7.5/150)\mathbf{L}$. Together with the mass m_1 of particle 1, this determines a maximal kinetic energy

$$E_{\max} := \frac{\hbar^2}{2m_1 d_1^2} \|\Delta\| = \frac{2\hbar^2}{m_1 d_1^2} \quad (94)$$

(see (27)). Writing this as

$$\frac{1}{2} m_1 v_{\max}^2$$

yields

$$v_{\max} = \frac{2\hbar}{m_1 d_1}. \quad (95)$$

In our example this computes to $\frac{150}{7.5 \cdot 7.5} 2 = 8.38$ which is indeed larger than the velocity $v = \pi$ to which we have boosted our Gaussian wave packet. Stated more generally: If a particle of mass m is to move with velocity v within a linear discrete biotope of geometrical length L , then we need at least

$$n = \frac{mvL}{2\hbar} \quad (96)$$

discretization points in this biotope. Notice that this represents n as a quotient of two angular momenta. This simple rule is the essential tool for adjusting the discretization to a given physical situation. The computational system can correspond to a physical system only if v is small compared to the velocity of light. Let us thus assume $v/c = 0.01$ from which we obtain the following relation between \mathbf{L} and \mathbf{T} :

$$\mathbf{T} = \frac{100\pi\mathbf{L}}{c} . \quad (97)$$

Consider for instance $\mathbf{L} = 1 \text{ nm}$. Then $\mathbf{T} = 1.048 \text{ fs}$, and $\mathbf{M} = 1.105 \cdot 10^{-31} \text{ kg}$. Therefore, $d_1 = 50 \text{ pm}$ and $m_1 = 8.288 \cdot 10^{-31} \text{ kg} = 0.1213 m_e$. The Compton wavelength $\hbar/(m_1 c)$ of particle 1 is by the factor 0.0085 smaller than the discretization length d_1 . This shows that concentration of the wave function to a single point is far from the degree of concentration which in a real system would lead to noticeable modification of the dynamics by field theoretic effects. However, there are peculiar effects with such strongly concentrated wave functions: The dynamics governed by the discrete Laplacian lets a very sharp Gaussian spread into two peaks (in one dimension) contrary to the normal spreading of Gaussian wave packets in which a single peak becomes wider and lower.

For particle 2, we only consider the transition between the ground-state and nearby excited states. Contrary to what we did for particle 1, we don't take over the shape of wave functions from continuum quantum mechanics. The number n_2 has to be large enough to let the eigenstates under consideration be sufficiently smooth and filling their biotope to a considerable fraction and nevertheless be practically zero at the rim of it. Varying this parameter under graphical feedback is a quite efficient method to achieve this. That here the value of n_2 is chosen as a power of 2 has no significance in the present context. It was useful in comparing eigenvalues and eigenvectors with those obtained from a treatment based on the Fast Fourier Transform.

5.2 Results from a typical simulation run

Most of the data to be shown here were created in a single program run of 2000 evolution steps which took 58.3 seconds. The time step $h = 0.00106798566$ was selected by the program by means of algorithm (80) aiming at satisfying criterion (60). For illustration of the scaling behavior (82) two further runs were needed with h is reduced to $h/2$ and $h/4$ respectively and, correspondingly, with 4000 and 8000 evolution steps.

Figures 2, 3, 4, and 5 should give an impression of the evolution of the 2-particle wave function during the main run. As mentioned already, Figure 2 is the initial state with particle 1 moving towards the center of the frame and particle 2 being in the oscillator



Figure 2: Initial state of the crossway system, $t = 0$

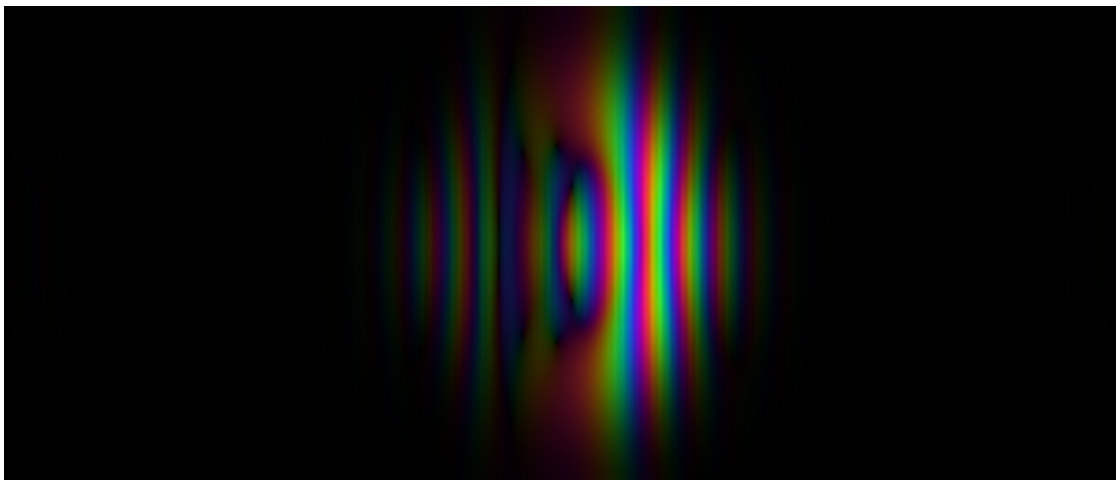
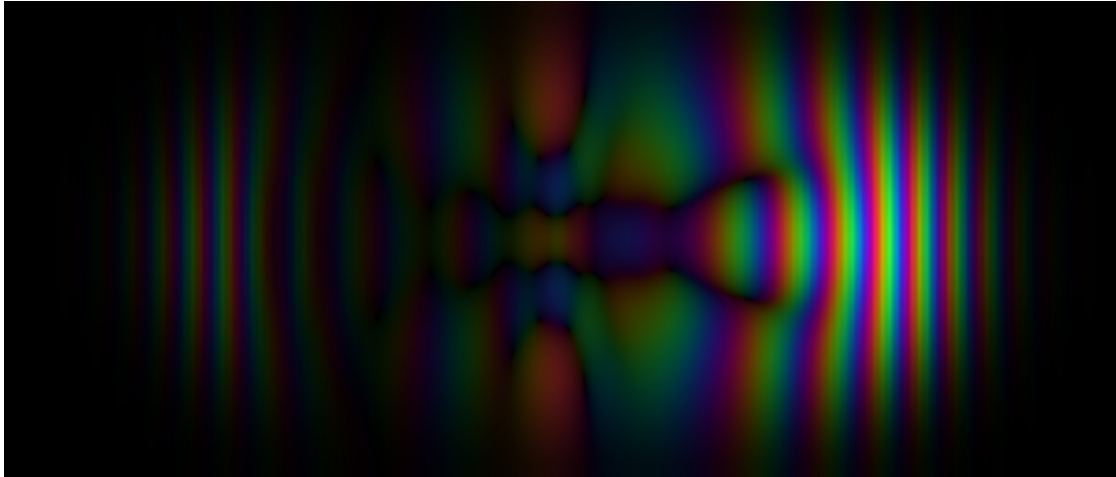
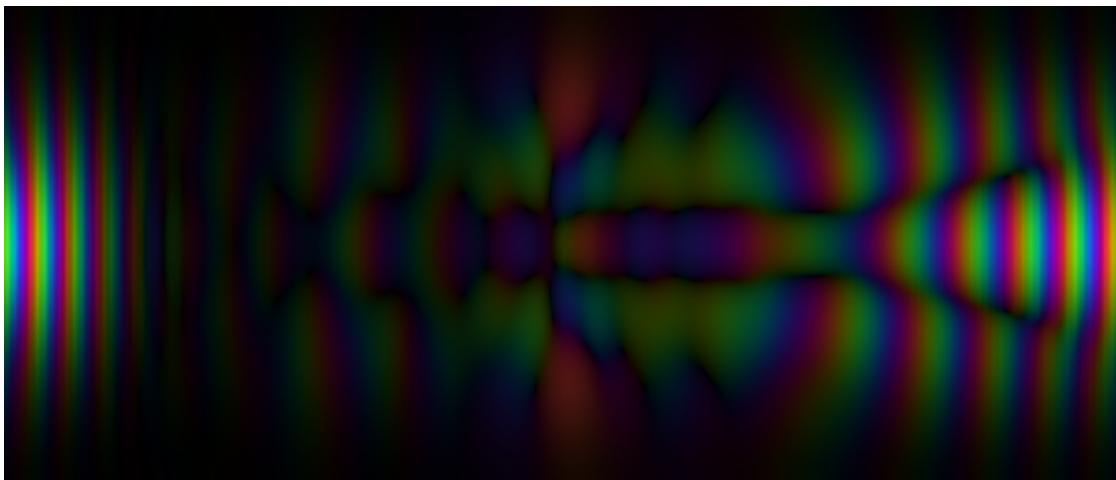


Figure 3: Interacting state of the crossway system, $t = 0.833$

ground state. At the center, interaction of the particles influences the wave function as shown in Figures 3 and 4. Figure 5 shows the wave function at the end of the present simulation run. Now there is a large amplitude for the situation that particle 1 has traversed its cyclic biotope and thus is seen at the left-hand side of the frame. Here, at the left-hand side of the frame, the wave function looks very much as in Figure 2, which says that particle 2 is still in the ground state. In a situations in which particle 2 is excited (visible as nodes of the wave function), particle 1 did travel less far. This is to be expected, since the energy for excitation has been taken from the kinetic energy of particle 1.

In the interaction zone, the wave function shows a rich structure. In some x-regions, the corresponding amplitude distribution in y-direction shows two nodes, in other x-

Figure 4: Scattering state of the crossway system, $t = 1.474$ Figure 5: Final state of the crossway system simulation, $t = 2.115$

regions we see four nodes. This indicates the predominance of the second and fourth excited state for particle 2 in situations characterized by particle 1 occupying the respective x-regions. It is certainly desirable to condense this complex information to a level that is more amenable to human comprehension. After much experimentation I devised a simple method which turned out to be very efficient in extracting interpretable features. The basic idea is to imitate destruction operators (which in the narrow technical sense don't apply since we don't have identical particles or a Fock space) to transform the two-particle state into a one-particle state. Precisely, we associate with any $\phi \in \mathcal{H}_{n_2}$

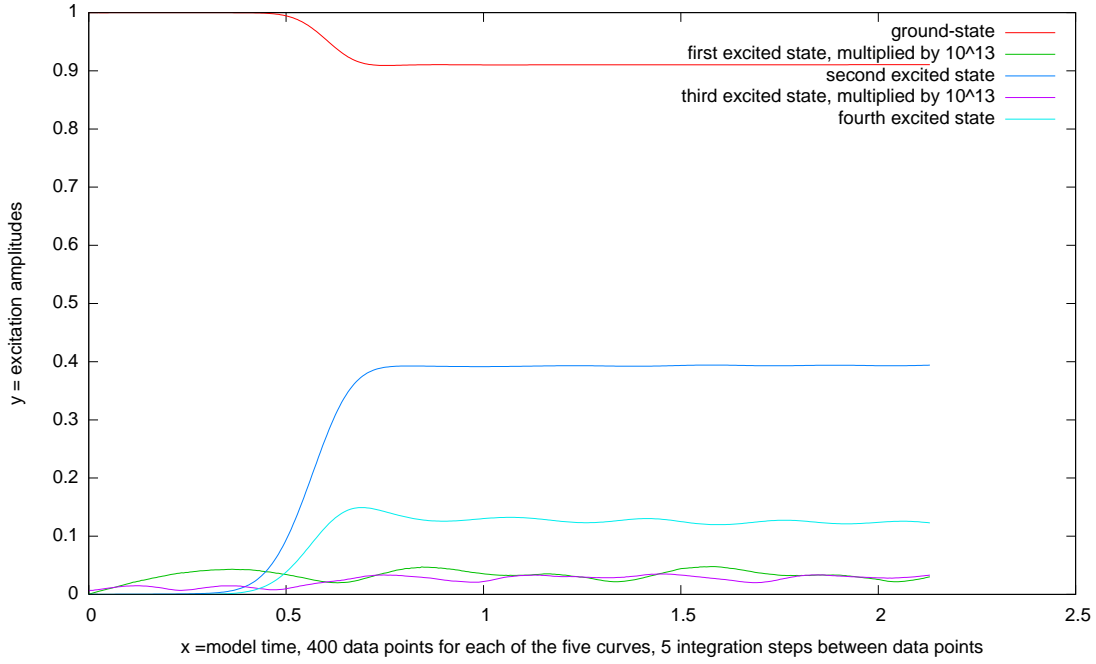


Figure 6: Excitation amplitudes

the operator $a(\phi) : \mathcal{H}_{n_1} \otimes \mathcal{H}_{n_2} \rightarrow \mathcal{H}_{n_1}$ as

$$(a(\phi)\psi)_i := \sum_{j=0}^{n_2-1} \psi_{ij} \bar{\phi}_j. \quad (98)$$

As the states to be destructed, there is here no other natural choice than choosing the energy-eigenstates ϕ_n , $n \in \{0, 1, 2, 3, 4\}$, which can be reached energetically by slowing down particle 1. For ψ we take, of course, the state of the crossway system as it evolves during the simulation. Then also the one-particle states $a(\phi_n)\psi$ evolve and can be visualized. Especially convenient is to use the 2-particle visualization capability with ψ replaced by the untangled auxiliary state $(a(\phi_n)\psi) \otimes \phi_n$. Here, it may suffice to show how the norm of these states

$$a_n(\psi) := \|a(\phi_n)\psi\|, \quad (99)$$

evolves during the simulation. These quantities will be referred to by the ad-hoc name *excitation amplitudes* and are represented in Figure 6 over the whole run. As the word amplitude suggests, the square of this quantities is a probability, namely the probability for finding the energy of particle 2 equal to the energy ε_n of state ϕ_n . The standard method to arrive at this probability is to define the projector $P_n = \mathbf{1} \otimes |\phi_n\rangle\langle\phi_n|$ and the expectation value $\langle\psi|P_n\psi\rangle$. Following this method one thus never encounters a wave function of particle 1 which is associated with the wave functions ψ and ϕ_n .

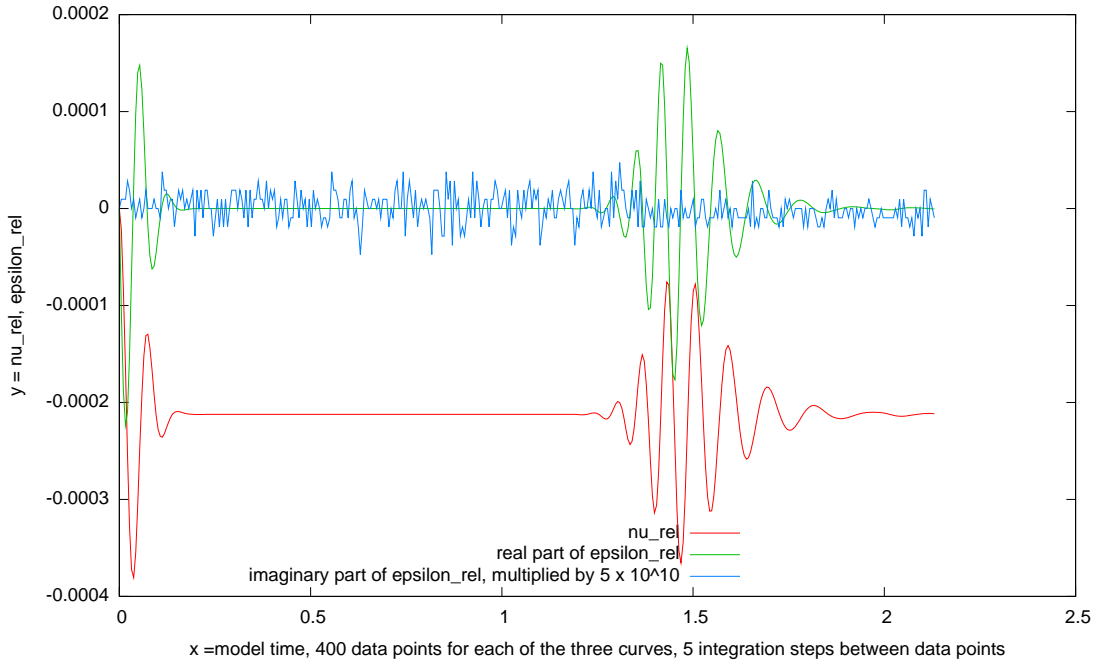
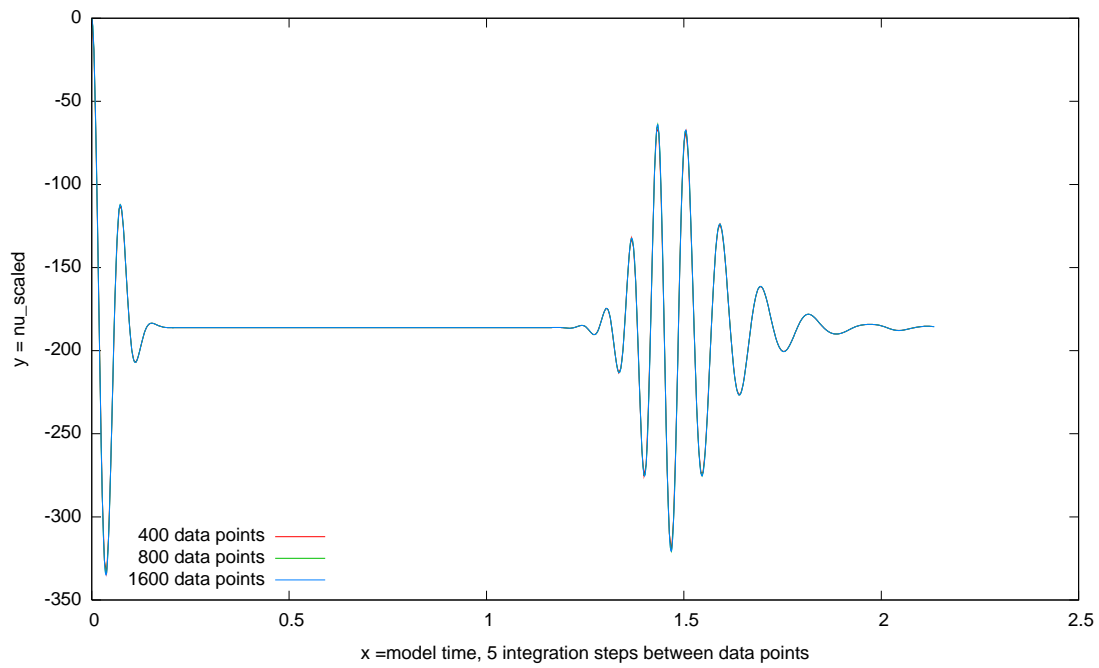
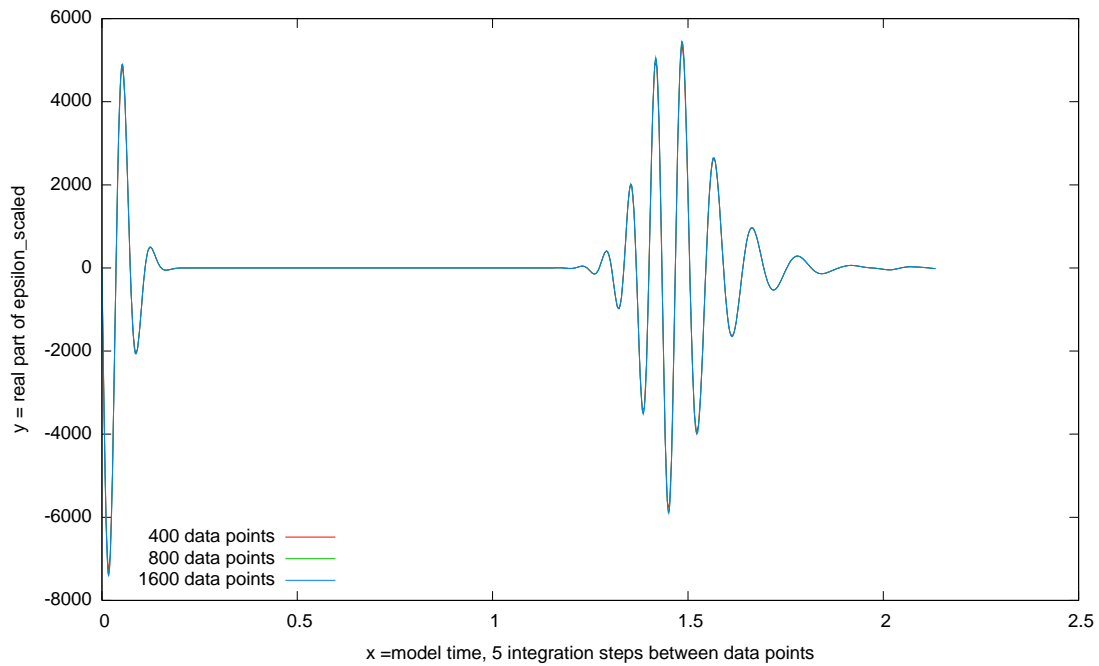


Figure 7: ν_{rel} and ϵ_{rel} for the main run of the crossway system

The curves clearly indicate the excitation of particle 2 from the ground state ϕ_0 to state ϕ_2 , and, with lower intensity, to the just reachable state ϕ_4 . Excitation to states ϕ_1 and ϕ_3 is forbidden by parity conservation. Actually, there is an extremely weak excitation, as the magnification factor shows, which is needed to make the corresponding curves visible in the diagram. As their smooth character indicates, these curves are not mere numerical noise. If one continues the simulation run, one finds a second shift of the excitation levels as particle 1 ‘passes the crossing again’, due to the torus topology of its biotope.

The Figure 7 is fully explained with equation (71) and the discussion in Section 4.3. The same is essentially true for Figures 8 and 9. For Figure 8 we can discuss the consequences of (83). The program computes $\|H\| = 1190$ and $\|H\psi\| = 38.5885$ for the initial state ψ , where, of course, $\|\psi\| = 1$. From the original data of the figure (for each of the three curves) one reads for all $t \in [0.31, 1.1]$ the constant value $\tilde{v}(\psi, t) = -186.134$ without exception. This is the constant level that according (83) should equal $-\frac{1}{8} \|H\psi\|^2$. This turns out to hold perfectly. The first minimum in \tilde{v} can be seen from the original data for $t_{\min} = 0.0360445$ which says $\epsilon_{\max} \approx \frac{\pi}{t_{\min}} = 43.67$ which has to be larger than $\|H\psi\|$ which is the case. The time t_{\min} is the time for a half-wave of wave $t \mapsto \cos 2e_{\max}t$. In the total time span 2.1358 we have 29.63 full waves of this frequency. This wave can be seen most clearly in the second burst shown in the figure. The dynamically relevant wave $t \mapsto \exp(i e_{\max}t)$ has only half this frequency so that we have 14.81 full waves in the whole run. Since the whole run consists of 2000 computed steps there are 135.01 computed steps per shortest wavelength. The maximum of h compatible with stability

Figure 8: v_{scaled} superposed from three runs of the crossway systemFigure 9: ϵ_{scaled} superposed from three runs of the crossway system

is π steps per shortest wavelength, so that a safety factor of 43 seems to have built in. Actually, increasing the step by a factor 1.57 makes the solution explode. The reason for this is a very small component of ψ with energies up to $\|H\|$ as discussed already near equation (80). Notice that these energies are 27 larger than those which determine the obvious wave structure of curve \tilde{v} . One will never notice this tiny high energy contribution if h is small enough to forbid this contribution to grow. That we see the shortest wave only in bursts, with calm regions in between, results from the interplay of broadening and traveling of the Gaussian wave packet. It is not related to interaction of the particles and also not to the energy levels of particle 2.

6 Conclusion

The present treatment of computational quantum dynamics comes close to satisfying for this particular problem what I consider a natural task for computational physics: Find for those basic notions of theoretical physics that are concerned with evolution of systems in time the programmable versions which execute effectively without making use of structures outside the basic physical framework. In our example of quantum dynamics this means that the Hamilton operator has to enter as an object that acts on states and by no functionality else.

I found this task amenable for celestial mechanics, rigid body dynamics, the dynamics of granular media, non-relativistic quantum dynamics of n-body systems interacting by pair potentials, and I expect that relativistic wave mechanics can be treated along these lines.

My impression is that C++ is the programming language that comes closest to the needs of such an enterprise. The strong points of C++ here are: templates, operator overloading, standard containers, and lambda abstraction (provided by some library).

Acknowledgments

I thankfully remember discussions with the late Professor Fritz Bopp who explained his vision concerning quantum mechanics in finite dimensional spaces. I'm grateful to many of my former industry colleagues, who helped me to become a productive programmer. Particularly, these were Rainer Braendle, Dieter Horlacher, Martin Landis, and Thomas Dera. Finally, I acknowledge furthering discussions with Felix Lev on Galois Fields in quantum theory.

References

- [1] U. Mutze: Relativistic quantum mechanics of n-particle systems with cluster-separable interactions, Phys. Rev. D, Vol. 29, 2255-2269, 1984
- [2] Felix Lev: Quantum Theory over a Galois Field and Spin-statistics theorem hep-th/0209001

-
- [3] Ulrich Mutze: Predicting Classical Motion Directly from the Action Principle II, Mathematical Physics Preprint Archive 1999–271
www.ma.utexas.edu/mp_arc/c/99/99-271.pdf
- [4] Ulrich Mutze: A Simple Variational Integrator for General Holonomic Mechanical Systems, Mathematical Physics Preprint Archive 2003–491
www.ma.utexas.edu/mp_arc/c/03/03-491.pdf
- [5] Ulrich Mutze: Rigidly connected overlapping spherical particles: a versatile grain model, *Granular Matter* Vol. 8, 185-194, 2006
- [6] William H. Press, Saul A. Teukolsky, William T. Vetterling, Brian P. Flannery: *Numerical Recipes in C*, Second Edition, Cambridge University Press 1992
- [7] www.maths.tcd.ie/~plynch/SwingingSpring/doublespring.html
- [8] DoRon B. Motter: Reversible Simulation and Visualization of Quantum Evolution
www.cise.ufl.edu/research/revcomp/Motter-sch/short-report.pdf
- [9] Werner O. Amrein, Josef M. Jauch, Kalyan B. Sinha: *Scattering Theory in Quantum Mechanics*, Benjamin 1977